IJNRD.ORG ISSN : 2456-4184
INTERNATIONAL JOURNAL OF NOVEL RESEARCH AND DEVELOPMENT (IJNRD) | IJNRD.ORG
An International Open Access, Peer-reviewed, Refereed Journal

Entropy Generation in Casson Fluid Flow Past a Stretching Plate

Preeti*

Department of Mathematics, KLP College, Rewari, Haryana, India

Email: preetirewaria25@gmail.com

Abstract

Entropy generation in a Casson fluid flow past a stretching plate is investigated by this paper. In thermodynamic process, Entropy generation is a measure of irreversibility factors. In heat transfer studies, it is a common feature. Also, such type of study includes the effect of viscous dissipation. By using the spectral local linearization method, we solve the model equations. The impact of some other physical parameters like the Casson, velocity, and temperature parameters are considered by the study. When we compare present results with published literature, a good correlation is achieved. The results of this show that the velocity parameter significantly effects the fluid flow, temperature profiles. Also, when the Casson parameter increases, the temperature profiles increase, whereas there is reduction in the velocity profile.

Keywords: Casson fluid; Entropy generation; Stretching plate.

INTRODUCTION: -

The concept of Nanofluids was introduced by Choi [8]. He proposed that nanoparticles be suspended in a certain base fluid such as oil, water, kerosene and ethylene glycol in his pioneer work on nanofluids. A nanofluid is a type of fluid that contains a suspension of nanoparticles. The assumption is that the nanoparticles are uniformly and stably distributed in a base fluid. Some unique nanofluid features were pointed outby Des et al. [10]. These features are theabnormal enhancement of thermal conductivity, stability, particle size dependence. The increase in the thermal conductivity of nanofluids was explained by Buongiorno [6]. A model, introduced by him, took into account the particle Brownian motion and thermophoresis diffusion. Buongiorno's model was used by Researchers and their studied nanofluid flows with the magnetic field, thermal radiation, nscous dissipation, porosity, and stability. The effect of parial slip(that is, the Navier's condition) on the boundary layer flow and heat transfer of nanofluids past a stretching sheet was investigated by Noghrehabadi et al. [30].The observation is that the slip of parameter strongly influences the flow velocity,

and the surface shear stress on the stretching sheet. There is a decrease in the momentum boundary layer thickness and an increase in the thermal boundary layer thickness.

The problem of laminar fluid flow was investigated numerically by Khan and Pop [18], which result from the stretching of a flat surface in a nanofluid. The effect of Brownian motion and thermophoresis diffusion was included in that model which he studied. The reduced Sherwood number increased with the parameters considered in the study was found them. The boundary layer flow in a nanofluid using a convective heating boundary condition was studied by Makinde et al. [22]. Their result is that for fixed values of the Prandti, Lewis, and Biot numbers, the local temperature rises as the Brownian motion, thermophoresis effects intensify. However, the temperature distribution is slightly affected when the Prandti number, Brownian motion, thermophoresis diffusion, and Biot number are fixed. Heat transfer in an incompressible viscous nanofluid flow past a semi-infinite vertical stretching sheet in the presence of a magnetic field was examined by Hamad [15].

The Casson fluid is that fluid which is a non-Newtonian fluid. Casson fluid can be defined as a shear thinning liquid that is assumed to have an infinite viscosity at zero rates of shear, yield stress below which no flow occurs and a zero viscosity at an infinite rate of shear, Dash et al. [11]. The behavior of it like an elastic solid at low shear strain, and it behaves like a Newtonian fluid above a critical stress value. There are some examples of Casson fluid such as tomato, honey, and human blood [26]. Recently, studies in Casson nanofluid have become popular. [27] carried out an analysis on Casson nanofluid flow past a non-linearly stretching sheet with magnetic field effects. Their conclusion is that Brownian motion has a negligible impact on temperature and heat transfer rate on the sheet; also, the skin friction coefficient values for the Casson fluid are greater than those of the Newtonian fluid.

The diffusion of chemically reactive species in Casson fluid flow over an unsteady stretching surface was analyzed by Makanda et al. [21]. It is observed by them that with an increase in magnetic and permeability parameters, the velocity profiles decrease, and the skin friction increases. On the contrary, the rate of heat as well as the concentration profiles, are decreased. The flow, heat, and mass transfer behavior in a Casson fluid flow past an exponentially permeable stretching surface was examined by Raju et al. [34]. Magnetic field effects,thermal radiation, viscous dissipation, heat source and chemical reaction were included in their study. Chemical reaction and magnetic field parameters, tend to minimize the skin friction coefficient was shown by them. The combined effects of Soret and Dufour numbers on the fluid flow, heat, and mass transfer of a Casson nanofluid over an unsteady stretching sheet with thermal radiation and heat generation was studied by Oyelakin et al. [32].

The problem of natural convective boundary layer flow of a nanofluid past a vertical plate, including the effects of Brownian motion and thermophoresis diffusion was revisited by Kuznetsov and Nield [20]. New model of them was argued that the nanofluid particle on the boundary should be passive rather than activity controlled to have a more realistic model.

A new mechanism is that mechanism which produces wall-parallel Lorentz force. This mechanism was developed by [12]. An electromagnetic actuator was proposed by them. It consists of permanent magnets and electrodes scaled on a plane surface. The setup is known as Riga-plate. The benefit of this setup is that it prevents boundary layer separation and reduces turbulence effects. In addition, it diminishes pressure drag and friction in submarines. [3,4] has studied mixed convective nanofluid flow bounded by a convectively heated vertical Riga-plate. On the contrary, [16] studied the flow of a nanofluid past a convectively heated Riga-plate with variable thickness.

Entropy generation has been associated with thermodynamic irreversibility a common feature is most heat transfer process. Fluid flow heat and mass transfer and entropy generation in a study Casson nanofluid flow past a stretching sheet with velocity slip and connective boundary condition was studied by [2]. [33], studied entropy generation on MHD Casson nanofluid flow over a porous stretching/shrinking surface. The influence of nonlinear thermal radiation and chemical reaction was included in their study. [1], investigated entropy generation on nanofluid flow through a horizontal Riga-plate. [5], studied entropy generation in unsteady two-dimensional squeezing flow between two Riga-plates. A Cattaneo Christov heat flux model and a convective boundary condition was included in their study.

Recently, entropy generation in a Casson nanofluid radiative flow was examined by Oyelakin and Sibanda [31]. Thermophoretic diffusion at the solutal boundary was assumed by them. Also, it was shown that the entropy generation number increases with increment in temperature difference. A significant source for entropy generation is irreversibility of heat transfer. [19], investigated entropy generation on double diffusive nanofluid flow with activation energy. The entropy generation diminishes by the dynamic viscosity of fluid used in the study was observed by [13] [14].

Much consideration to the best of the author's knowledge has not given the study of entropy generation in a Casson nanofluid flow past an electromagnetic stretching Riga sheet. The aim of this paper is to study the fluid flow, heat transfer, mass transfer, and entropy generation effects in a Casson nanofluid flow on an electromagnetic sheet. The traditional Casson nanofluid model is revised. It has been revised to include the impact of the electromagnetic parameter. We use the spectral local realization method which was proposed by Motra [24] to solve the model equations. The spectral local linearization method has the quirk of fast convergence and good accuracy, which has been shown in some recent studies [35,7]. This study has a wide application in numerous industrial discipline such as the cooling of electric devices, transportation,etc.

MathematicalFormulation:-

Let us consider a coordinate system that originate from the leading edge of the Riga plate. We focus on the Buongiorno model in this study, which considers the Brownian motion and thermophoresis diffusion of nano particles. Moreover, the influence of viscous dissipation is considered in the flow. It is given that u and v are the components of velocity in the direction of x and y respectively. Here, x-axis is assumed to be along the sheet, and the y-axis is perpendicular to it, which is shown n figure 1: -

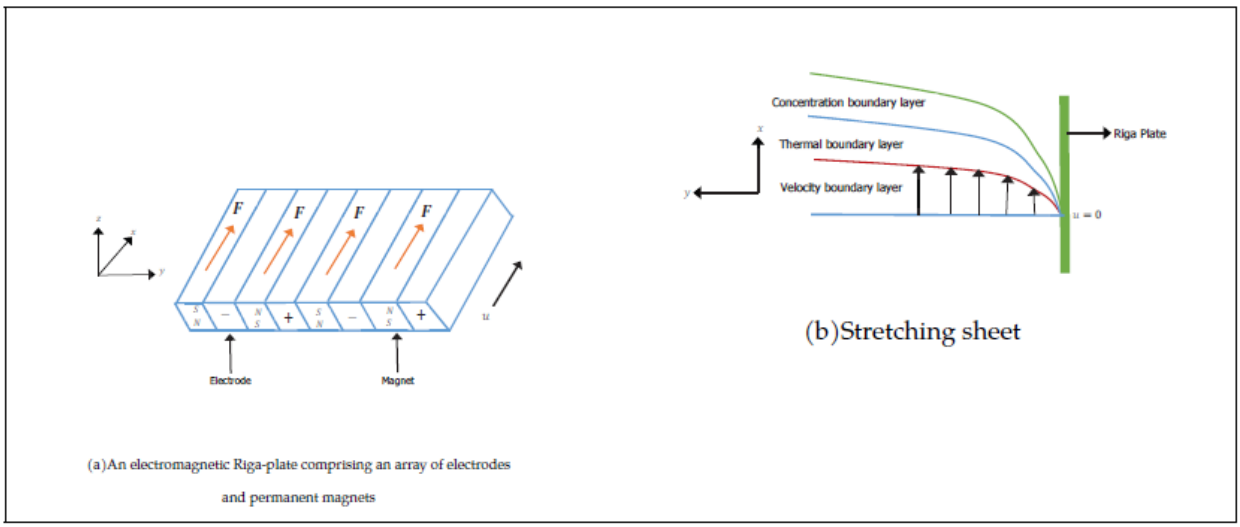

Figure-1 Physical configuration and coordinate system of the problem.

An electromagnetic field which is produced by Riga plate, creates a wall parallel to Lorentz force of exponentially decaying nature. We denote the velocity at the ambient fluid by $u_\infty(x) = cx$, where c is a positive constant. Let us use the assumptions defined above, the boundary layer equations are [17].

$$\frac{\partial u}{\partial x} + \frac{\partial v}{\partial y} = 0 \tag{1}$$

$$u\frac{\partial u}{\partial x} + v\frac{\partial u}{\partial y} = u_\infty \frac{du_\infty}{dx} + \frac{\mu_f}{\rho_f}\left(1 + \frac{1}{\beta}\right)\frac{\partial^2 u}{\partial y^2} + \frac{\pi j_{0M_0}}{8\rho_f} e^{-\left(\frac{\pi}{\Delta}\right)y} \tag{2}$$

$$u\frac{\partial T}{\partial x} + v\frac{\partial T}{\partial y} = \frac{k_f}{(pc_f)}\frac{\partial^2 T}{\partial y^2} + \tau\left[D_B\frac{\partial C}{\partial y}\frac{\partial T}{\partial y} + \frac{D_T}{T_\infty}\left(\frac{\partial T}{\partial y}\right)^2\right] + \frac{\mu_f}{(\rho c_p)_f}\left(1 + \frac{1}{\beta}\right)\left(\frac{\partial u}{\partial y}\right)^2 \tag{3}$$

$$u\frac{\partial C}{\partial x} + v\frac{\partial C}{\partial y} = D_B\frac{\partial^2 C}{\partial y^2} + \frac{D_T}{T_\infty}\frac{\partial^2 T}{\partial y^2} \tag{4}$$

The associated boundary conditions are,

$$u = u_w(x) = ax,\ \ v = 0,\ \ T = T_w\ ,\ \ C = C_w\ \ as\ y = 0 \tag{5}$$

$$u \to u_\infty(x) = Cx,\ \ T \to T_\infty\ ,\ \ C \to C_\infty\ \ as\ y \to \infty \tag{6}$$

Where, u and v are the velocities in the x and y directions respectively. Here, B is the Casson number C and T are solutal concentration and temperature respectively. The heat capacity of the fluid be $\tau = \in \frac{(\rho c)_P}{(\rho C)_f}$ with $(\rho c)_f$ and $(\rho c)_P$ are the effective heat capacity of the nano particle material. The Brownian diffusion coefficient is D_B and thermophoresis diffusion coefficient is D_T . The density of the fluid is ρ, the density of current is j_0 and the magnetization of magnets is M_0 .We have to transform the partial differential equations into a system of ordinary differential equations, let us introduce the following dimensionless variables.

$$\varphi = \sqrt[x]{av_f}\, f(x)\ ,\ \ n = \sqrt{\frac{a}{v_f}}\, y\ ,\theta(n) = \frac{T - T_\infty}{T_w - T_\infty}\ ,\qquad \emptyset(n) = \frac{C - C_\infty}{C_w - C_\infty} \tag{7}$$

Using the stream function equations,

$u = axf'(x)$ and $v = -\sqrt{av_f}f(x)$,

The continuity equations in (1) is readily satisfied and the dimensionless form equation (2)-(4) become,

$$\left(1 + \frac{1}{\beta}\right)f''' + ff'' - f'^2 + ze^{-n^2} + \in^2 = 0, \tag{8}$$

$$\frac{1}{P_r}\theta'' + f\theta' + \left(1 + \frac{1}{\beta}\right)Ecf''^2 + Nb\emptyset'\theta' + Nt\theta'^2 = 0, \tag{9}$$

$$\emptyset'' + Lef\emptyset' + \frac{Nt}{Nb}\theta'' = 0, \tag{10}$$

And the corresponding dimensionless boundary conditions become:

$$f(0) = 0, f'(0) = 1, \theta(0) = 1, \emptyset(0) = 1, \tag{11}$$

$$f'(\infty) \to \varepsilon, \theta'(\infty) \to 0, \emptyset'(\infty) \to 0, \tag{12}$$

Where $P_r = \frac{v_f(\rho c_P)_f}{K_f}$ is the Prandti number, $Le = \frac{V_f}{D_B}$ is the Lewis number, $N_b = \frac{\tau D_B}{V_f}(c_w - c_\infty)$ is the Brownian motion parameter, $N_t = \frac{\tau D_T}{V_f T_\infty}(T_w - T_\infty)$ is the thermophoresis parameter,$\in = \frac{c}{a}$ is the velocity ratio parameter, $z = \frac{\pi M_0 j_0 x}{8\rho {f_w}^{\mu^2}}$ is the modified Hartmann number, $\delta = \frac{\pi}{\sqrt{\frac{a}{V_f}}}$ is the width parameter, $E_c = \frac{{\mu_w}^2}{c_{P(T_w - T_\infty)}}$ is the local Eckert number.

The skin friction coefficient, the local Nusselt number coefficient and the local Sherwood number coefficient are given as,

$$Cf_x = \frac{\tau_w}{\rho f {\mu_w}^2}, N\mu_x = \frac{q_0 x}{k_f(T_w - T_\infty)}, Sh_x = \frac{q_m x}{D_B(c_w - c_\infty)}, \tag{13}$$

where,

$$T_w = \left(\mu_\beta + \frac{\rho_y}{\sqrt{2\pi_c}}\right)\mu_f \frac{\partial u}{\partial y}\Big|_{y=0}, \quad q_w = -k_f \frac{\partial T}{\partial y}\Big|_{y=0}, \quad q_m = -D_B \frac{\partial c}{\partial y}\Big|_{y=0}, \tag{14}$$

Putting these values of (14) into (13); we get,

$$Cf_x = \frac{\mu_f}{\rho f {\mu_w}^2}\left(1 + \frac{1}{\beta}\right)\frac{\partial u}{\partial y}\Big|_{y=0}, N\mu_x = -\frac{x}{(T_w - T_\infty)}\frac{\partial T}{\partial y}\Big|_{y=0},$$
$$Sh_x = -\frac{x}{(c_w - c_\infty)}\frac{\partial C}{\partial y}\Big|_{y=0}, \tag{15}$$

Now, putting values of (7) into (15), we get

$${Re_x}^{1/x} Cf_x = \left(1 + \frac{1}{\beta}\right) f''(0), {Re_x}^{1/2} N\mu_x = -\theta'(0), {Re_x}^{-1/2} Sh_x = -\emptyset'(0), \tag{16}$$

Where $Re_x = {\mu_w}^x/_{v_f}$ is known as the Reynolds number.

Entropy Generation Analysis: -

[5] expresses the entropy generation for the Casson nanofluid.

$$S_{gen} = \frac{k_f}{{T_\infty}^2}\left(\frac{\partial T}{\partial y}\right)^2 + \frac{\mu_f}{T_\infty}\left(1 + \frac{1}{\beta}\right)\left(\frac{\partial u}{\partial y}\right) + \frac{RD_B}{c_\infty}\left(\frac{\partial C}{\partial y}\right)^2 + \frac{RD_B}{T_\infty}\left(\frac{\partial T}{\partial y}\frac{\partial C}{\partial y}\right) \tag{17}$$

From equation (17), we get;

The first term is due to heat transfer, the second term is due to fluid friction, and the third term is due to mass transfer. Now, the characteristic entropy generation is defined as,

$$S_0 = k_f \frac{(T_w - T_\infty)^2}{{T_\infty}^2 x^2} (18)$$

Using the similarity transformations, which are defined in equation (7), the entropy generation in dimensionless form is written as,

$$N_G = \frac{S_{gen}}{S_0} = Re\theta'^2 + \frac{B_r Re}{\Omega}\left(1 + \frac{1}{\beta}\right) f''^2 + \lambda_1 Re \left(\frac{x}{\Omega}\right)^2 \emptyset'^2 + \lambda_1 Re \left(\frac{x}{\Omega}\right) \theta'\emptyset', \quad (19)$$

Where Re is the Reynold's number, B_r is the Brinkmann number, Ω is the dimensionless temperature, λ_1 is the diffusion coefficient and x is the dimensionless Concentration; which are defined as,

$$Re = \frac{u_w x}{v_f}, B_r = \frac{u_f {u_w}^2}{k_f (T_w - T_\infty)}, \Omega = \frac{(T_w - T_\infty)}{T_\infty}, \lambda_1 = \frac{R D_B C_\infty}{k_f}, x = \frac{(C_w - C_\infty)}{C_\infty}, \quad (20)$$

In irreversibility studies, a ratio of the heat transfer irreversibility is termed the Bejan number and is defined as,

$$Be = \frac{Re\theta'^2}{Re\theta'^2 + \frac{B_r Re}{\Omega}\left(1 + \frac{1}{\beta}\right) f''^2 + \lambda_1 Re \left(\frac{x}{\Omega}\right)^2 \emptyset'^2 + \lambda_1 Re \left(\frac{x}{\Omega}\right) \theta'\emptyset'}, \quad (21)$$

These cases are examined for the Bejan number. Firstly, if $Be < 0.5$, this implies that the total irreversibility dominates. The second thing is that, if $Be > 0.5$, it means that the heat transfer irreversibility dominates. In the end, if $Be = 1$, it implies that the irreversibility results from the heat transfer only.

Method of Solution: -

We use the spectral local linearization method for solving the differential equations in (8)-(10), which are described by [23]. The spectral local linearization method has been used by researchers for solving mathematical model equations [28,39]. With a high accuracy level, the method has proved to be highly convergent. [23,37,36] describes the method in details. Corresponding to equations (8)-(10), the local linearization scheme is,

$$a_{0,r} f'''_{r+1} + a_{1,r} f''_{r+1} + a_{2,r} f'_{r+1} + a_{3,r} f_{r+1} = R_{1,r}, \quad (22)$$

$$b_{0,r} \theta''_{r+1} + b_{1,r} \theta'_{r+1} = R_{2,r}, \quad (23)$$

$$\emptyset''_{r+1} + C_{1,r} \emptyset'_{r+1} = R_{3,r}, \quad (24)$$

Where the subscript $r+1$ represents the current iteration and subscript r represent the previous iterations. The variable coefficients $a_{i,r}$, $b_{i,r}$ and $C_{i,r}$ $(i = 1,2,3, \dots)$ are defined as,

$$a_{0,r} = \left(1 + \frac{1}{\beta}\right), \quad a_{1,r} = f_r, \quad a_{2,r} = -2f_r', \quad a_{3,r} = f_r'''$$

$$b_{0,r} = \frac{1}{P_r}, \quad b_{1,r} = f_r + Nb\emptyset_r' + 2Nt\theta_r', \text{and} \quad C_{1,r} = Lef_r.$$

The righthand sides are given as,

$$R_{1,r} = a_{0,r}f_r''' + a_{1,r}f_r'' + a_{2,r}f_r' + a_{3,r}f_r - F_1, \tag{25}$$

$$k_{2,r} = b_{0,r}\theta_r'' + b_{1,r}\emptyset_r' - F_2, \tag{26}$$

$$R_{3,r} = \emptyset_r'' + C_{1,r}\emptyset_r' - F_3, \tag{27}$$

Where,

$$F_1 = \left(1 + \frac{1}{\beta}\right)f_r''' + f_r f_r'' - f_r'^2 + Ze^{-\eta\delta} + \varepsilon^2, \tag{28}$$

$$F_2 = \frac{1}{P_r}\theta_r'' + f_r\theta_r' + \left(1 + \frac{1}{\beta}\right)Ecf_r''^2 + Nb\emptyset_r'\theta_r' + Nt\theta_r'^2, \tag{29}$$

$$F_3 = \emptyset_r'' + Lef_r\emptyset_r' + \frac{Nt}{Nb}\theta_r''. \tag{30}$$

We solve the equations starting with the help of a given set of suitable initial approximations. The semi-infinite domain [0,∞] to a truncated domain $[0,l_\infty]$, where l_∞ is a number which is finite, also it is large enough to represent the flow conditions at ∞. Now, using a suitable linear transformation, $\eta \in [0, l_\infty]$ is transformed to $x \in [-1,1]$. The Chebyshev differentiation matrix D which is defined in [40], is introduced to estimate the derivatives of the unknown variables at the Collocation points as matrix vector product represented as,

$$\frac{df}{d\eta} = \sum_{j=0}^{N_x} D_{jk}\, f(x_j) = DF, \quad k = 0,1,2,\dots,N_x, \tag{31}$$

Where the number of collocation points is $N_x + 1$, $D = {}^{2D}/_{C_\infty}$ and

$F = [f(x_0), f(x_1), \dots, f(x_{N_x})]^T$ which is a vector function at the collocation points. As powers of D, higher order derivatives are obtained, that is,

$$\frac{d^s f}{d\eta^s} = D^s F, \tag{32}$$

Where the order of the derivative is S and the size of matrix D is $(N_x + 1) \times (N_x + 1)$. To define the nodes in [-1,1], the Gauss Lobatto points are chosen as,

$$x_i = \cos\frac{\pi i}{N_x}, \quad i = 0,1,\dots,N_x, \quad -1 \le x \le 1; \tag{33}$$

Applying (31) to the scheme in (22)-(24), the decoupled system may be expressed as,

$$\left(a_{0,r}D^3 + a_{1,r}D^2 + a_{2,r}D + a_{3,r}I\right)F_{r+1} = R_{1,r} \ , \tag{34}$$

$$\left(b_{0,r}D^2 + b_{1,r}D\right)\theta_{r+1} = R_{2,r} \ , \tag{35}$$

$$\left(D^2 + C_{1,r}D\right)\emptyset_{r+1} = R_{3,r} \ , \tag{36}$$

Where I is an $(N_x + 1) \times (N_x + 1)$ identity matrix, the diagonal matrices are represented by the bold variable coefficients.

In a more compact form,

$$A_1F_{r+1} = R_{1,r} \ ,$$

$$A_2\theta_{r+1} = R_{2,r} \ ,$$

$$A_3\emptyset_{r+1} = R_{3,r} \ . \tag{37}$$

Where,

$$A_1 = a_{0,r}D^3 + a_{1,r}D^2 + a_{2,r}D + a_{3,r}I \ ,$$

$$A_2 = b_{0,r}D^2 + b_{1,r}D \ ,$$

$$A_3 = D^2 + C_{1,r}D \ . \tag{38}$$

Results and Discussion: -

On the velocity temperature and concentration profiles, we discuss the significance of the parameters in this section. We solve the conservation equations by using the spectral local linearization method. We see that the result of this problem is similar trend to some previously works which are published in [9], [28], [38].

While keeping the other parameters fixed, figures 2-4 show the effect of Casson parameter on the velocity, temperature, and concentration profiles. It is also known in figure 2 that the velocity profile is decreasing, and as such, the momentum boundary layer thickness increases. In the figure 3, it is shown that increasing the Casson parameter enhances the temperature profile and increases the thermal boundary layer thickness. In the figure 4, the concentration profile is depicted, which increases with the Casson parameter due to an enhancement in the solutal boundary layer thickness.

The effect of velocity ratio parameter on the velocity temperature and concentration profiles is shown in figures 5-7. We note from figure 6, that the velocity profile decreases when the velocity ratio is less than unity. When we do comparison, we see that the velocity profile increase when the value of the velocity ratio is greater than unity. This is a similar trend to those which is obtained in [25]. From figures 6 and 7, it is clear that both temperature and concentration profiles are decreasing when the velocity ratio parameter is increasing.

The graphs of the velocity, temperature, and concentration profiles are illustrated in figures 8-10, when the modified Hartmann number is increased. From figure 8, it is noted that there is a significant increase in the velocity profiles. When we vary the modified Hartmann number, the Lorentz force effect is observed. Generally, resistance to the fluid flow is offered by the Lorentz force. In the Lorentz forces effect, the higher values of the modified Hartmann number lead to a decrease. Thus, we observe an increase in velocity distribution.

On temperature and concentration profiles, the effect of modified Hartmann number is shown in figures 9 and 10. From the figures, we can see that the temperature and the concentration profile is decreasing as the modified Hartmann number is increasing. This leads to a decrease in the thermal and also in solutal boundary layers. Behind such behavior, the reason is that an increase in the modified Hartmann number amplifies the Lorentz force, which resists the fluid motion. We observe a decrease in temperature and solutal distributions due to this resistance.

On the entropy generation, figures 11-16 portray the effect of appropriate parameters. Figure 11 depicts the influence of the Reynolds number R, on the entropy generation number N_G. Entropy generation is an increasing function of R. This shows that the enhancement in the entropy production is due to the dominance in the inertial forces, that is, the Reynolds number's higher values. From figure 12, it is clear that entropy generation increases with an increase in the Brinkmann number. Higher frictional heating is indicated in the system by the higher values of the Brinkmann number.

It is indicated by figure 13 that when the Casson parameter values increase, entropy generation deceases. Entropy generation decreases with the enhancement in modified Hartmann number is illustrated by figure 14. In the Hartmann number, an increase shows a stronger Lorentz force, the flow is restarted and the entropy generation is increased by this force. It is shown by the figure 15 that when the temperature decreases, entropy generation increases. In regions adjacent to walls, entropy is high. In some parts of the sheet, there is a lesser heat transfer due to vanishing temperature gradients. The impact of the dimensionless concentration X is depicted by figure 16. For a given value of η, as X increase, the entropy generation number N_G increases for fixed value of the dimensionless temperature Ω=1. This increase is because of the contribution of mass transfer to the entropy generation and this augmentation continues up to a certain value of η.

On some parameters, the impact of the Bejan number is shown in figures 17-20. We note an opposite trend to the behavior of the entropy generation number for all parameters considered. The reason behind it that the Bejan number is a fraction of the heat transfer irreversibility and the total entropy generation number. The behavior of these profiles shows that irreversibility is vary dominant because of that transfer and has a high impact on the Bejan number. The Bejan number decreases for higher values of the Brinkmann number and dimensionless concentration. Although, they concide after a certain value of the parameters which is shown in figures 17 and 21. It can be shown in figures 18 and 20, that Bejan number escalates with Casson parameter and dimensionless temperature. A different trend is observed for the modified Hartmann number in figure 19 up to a certain value of Z, Bejan number increases and then retards.

Tables and Figures: -

Table 1: Comparison of numerical results of $f''(0)$ and $\theta'(0)$ for different values of the velocity ratio parameter when $\delta = Z = Nt = Ec = 0, Pr = Le = 1, Nb \to 0$ and $\beta \to \infty$.

ϵ	$-f''(0)$		$-\theta'(0)$	
	Present	[28]	Present	[28]
0.10	-0.96939	0.96938	0.60215	0.60281
0.30	-0.84942	0.84942	0.64727	0.64732
0.80	-0.29939	0.29938	0.75709	0.75709
1.00	0.00000	0.00000	0.79787	0.79788
2.00	2.01750	-2.01750	0.97871	0.97872
3.00	4.72928	-4.72928	1.13207	1.13209

Table 2: Variations values of skin friction coefficient, Nusselt, and Sherwood numbers for different values of some parameters when $\delta = Z = 0.5, \epsilon = 0.1, Pr = 1, Nb = 0.3, Nt = 0.3, Le = 5; \beta = 2$, and $Ec = 0.1$.

Z	δ	Nt	ϵ	Ec	β	$\left(1+\frac{1}{\beta}\right) f''(0)$	$-\theta'(0)$	$-\phi'(0)$
0.00						−1.1873	0.4047	1.5307
0.50						−0.8121	0.4572	1.5824
1.00						−0.4639	0.4930	1.6253
	0.10					−0.6134	0.4974	1.6206
	0.20					−0.6783	0.4850	1.6083
	0.40					−0.7757	0.4650	1.5895
		0.10				−0.8121	0.4995	1.6326
		0.30				−0.8121	0.4572	1.5824
		0.50				−0.8121	0.4193	1.5586
			0.00			−0.8411	0.4496	1.5763
			0.30			−0.6844	0.4808	1.6043
			0.80			−0.0512	0.5496	1.6932
				0.00		−0.8121	0.4787	1.5683
				0.10		−0.8121	0.4572	1.5824
				0.50		−0.8121	0.3705	1.6390
					0.10	−2.6539	0.4664	1.6708
					2.00	−0.8121	0.4572	1.5824
					5.00	−0.7097	0.4540	1.5703

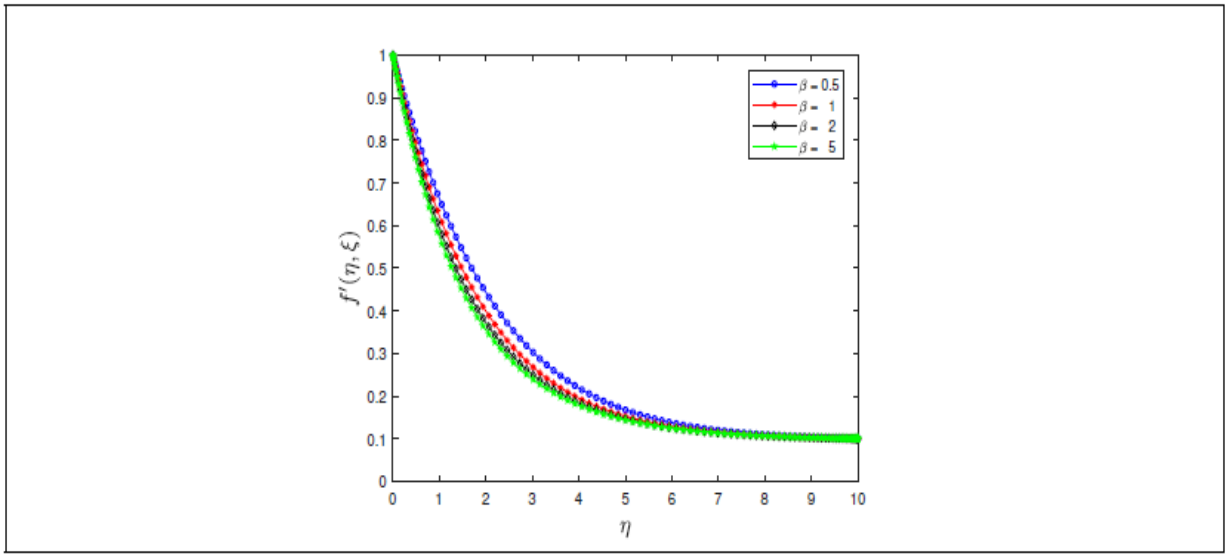

Figure 2: Effect of Casson fluid on the velocity profile when $\delta = Z = 0.5, \epsilon = 0.1, Pr = 1; Nb = Nt = 0.3, Le = 5$ and $Ec = 0.1$.

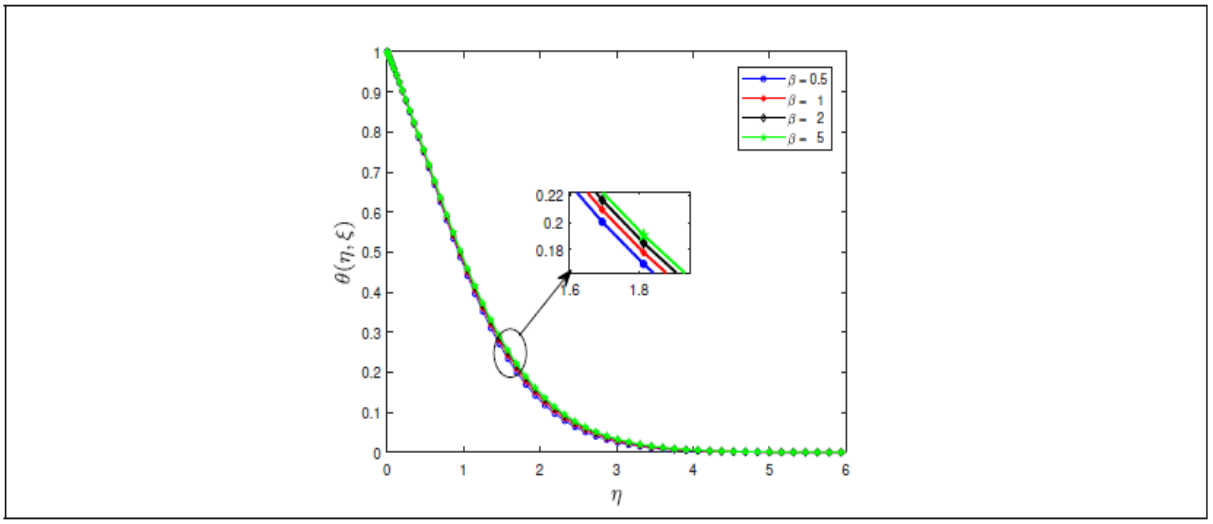

Figure 3: Effect of Casson fluid on the temperature profile when $\delta = Z = 0.5, \epsilon = 0.1, Pr = 1; Nb = Nt = 0.3, Le = 5$ and $Ec = 0.1$.

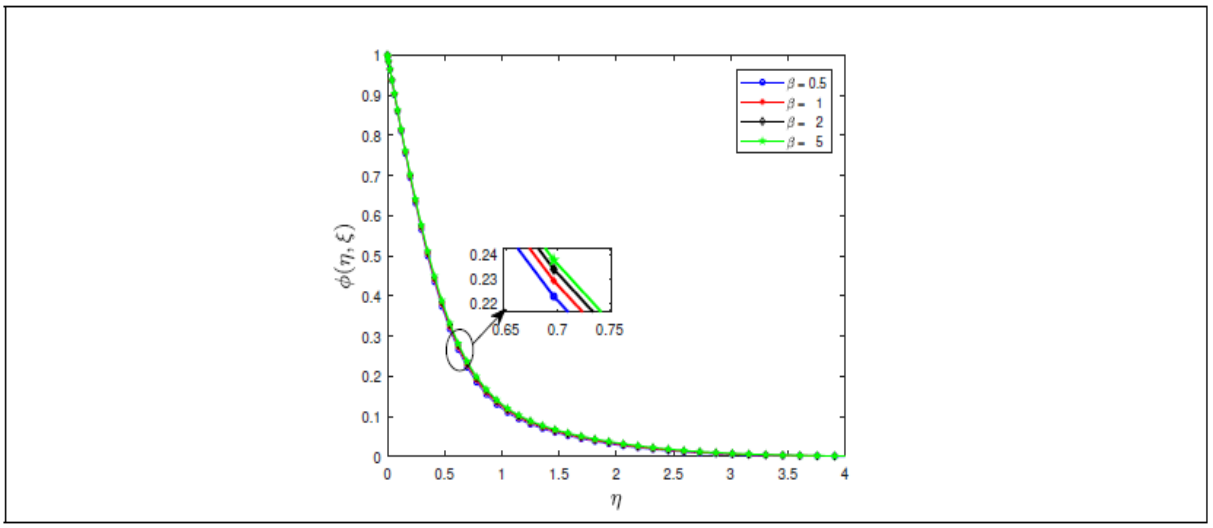

Figure 4: Effect of Casson fluid on the concentration profile when $\delta = Z = 0.5, \epsilon = 0.1, Pr = 1; Nb = Nt = 0.3, Le = 5$ and $Ec = 0.1$.

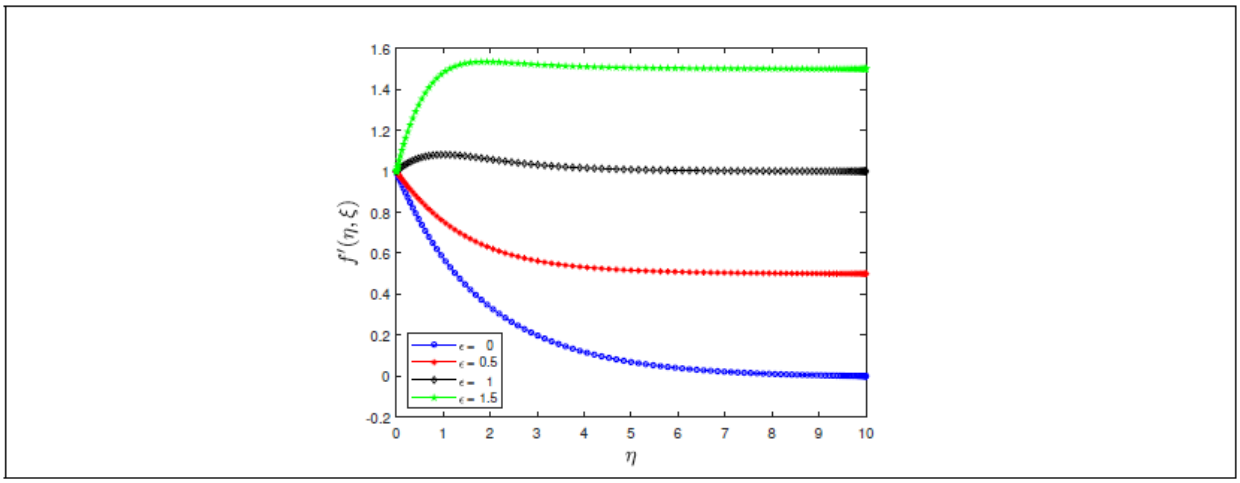

Figure 5: Effect of velocity ratio parameter on the velocity profile when $\beta = 2, \delta = Z = 0.5, Pr = 1; Nb = Nt = 0.3, Le = 5$ and $Ec = 0.1$.

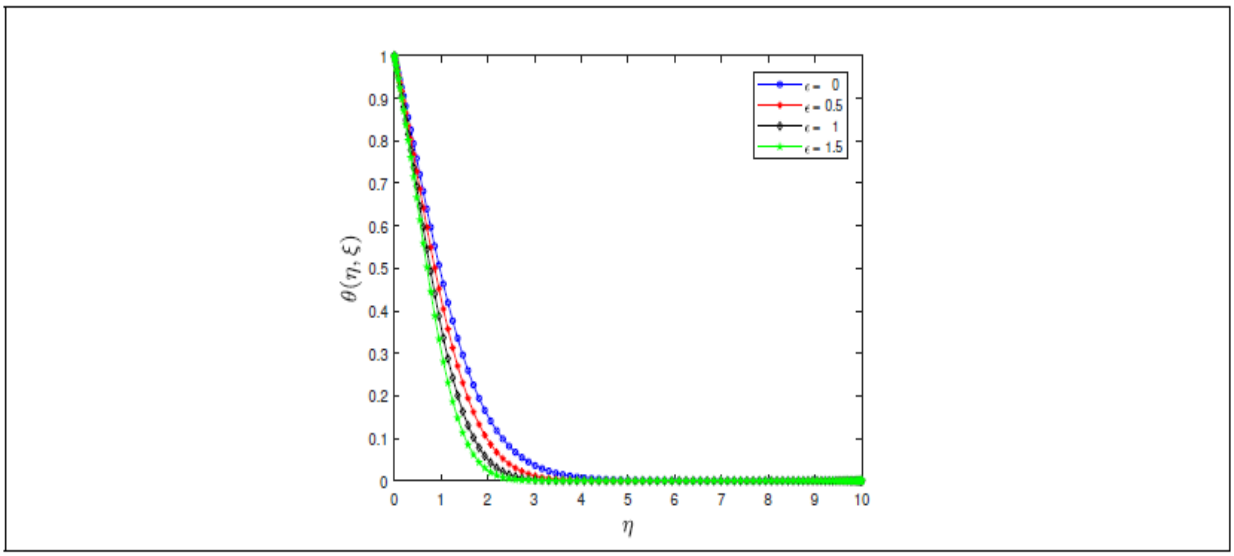

Figure 6: Effect of velocity ratio parameter on the temperature profile when $\beta = 2, \delta = Z = 0.5, Pr = 1; Nb = Nt = 0.3, Le = 5$ and $Ec = 0.1$.

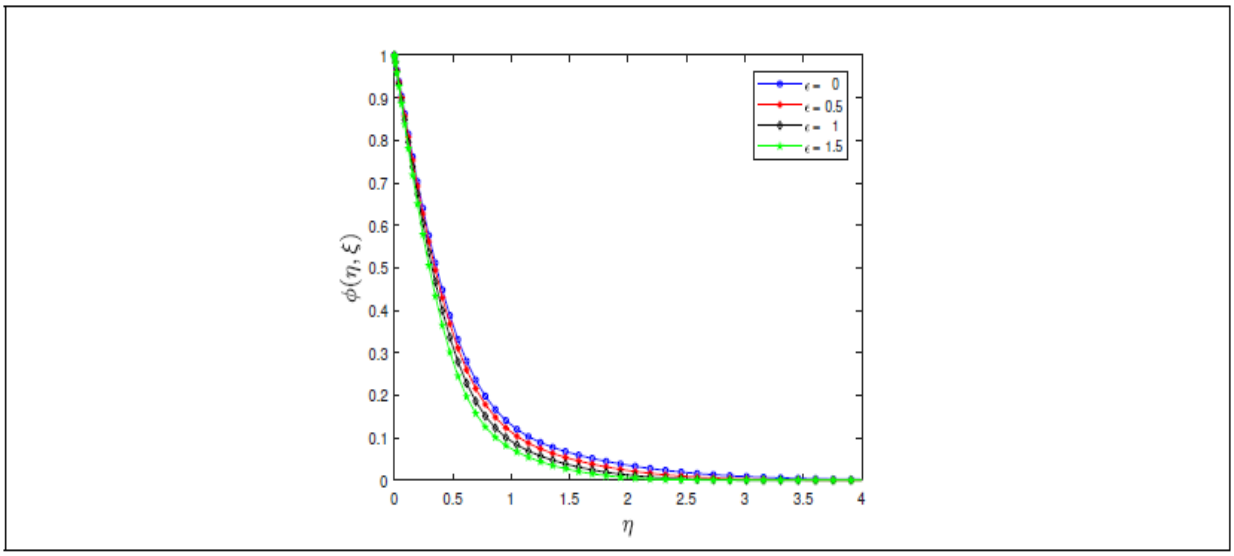

Figure 7: Effect of velocity ratio parameter on the concentration profile when $\beta = 2, \delta = Z = 0.5, Pr = 1; Nb = Nt = 0.3, Le = 5$ and $Ec = 0.1$.

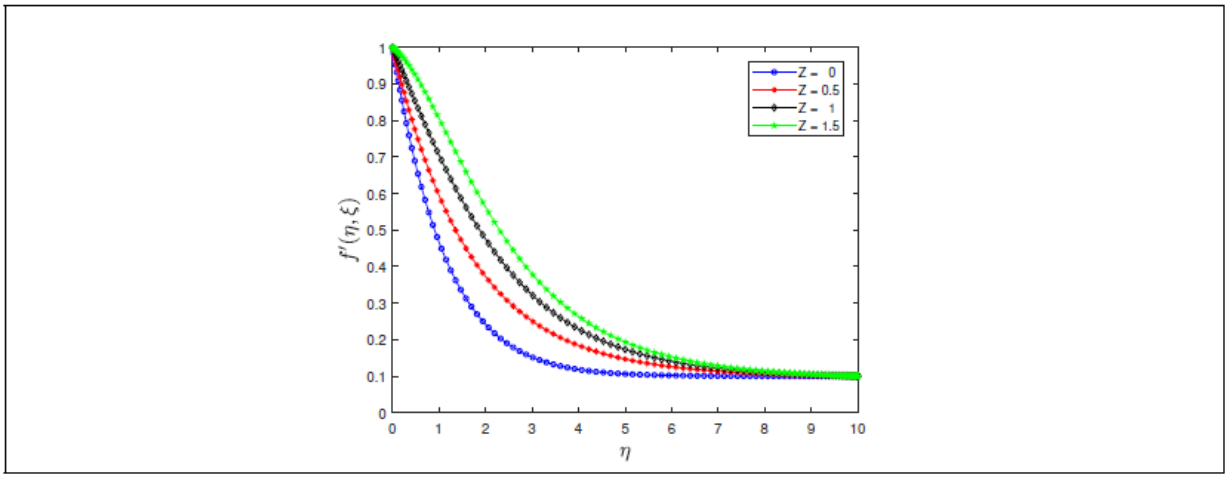

Figure 8: Effect of modified Hartmann number on the velocity profile when $\beta = 2, \delta = 0.5, \epsilon = 0.1, Pr = 1; Nb = Nt = 0.3, Le = 5$ and $Ec = 0.1$.

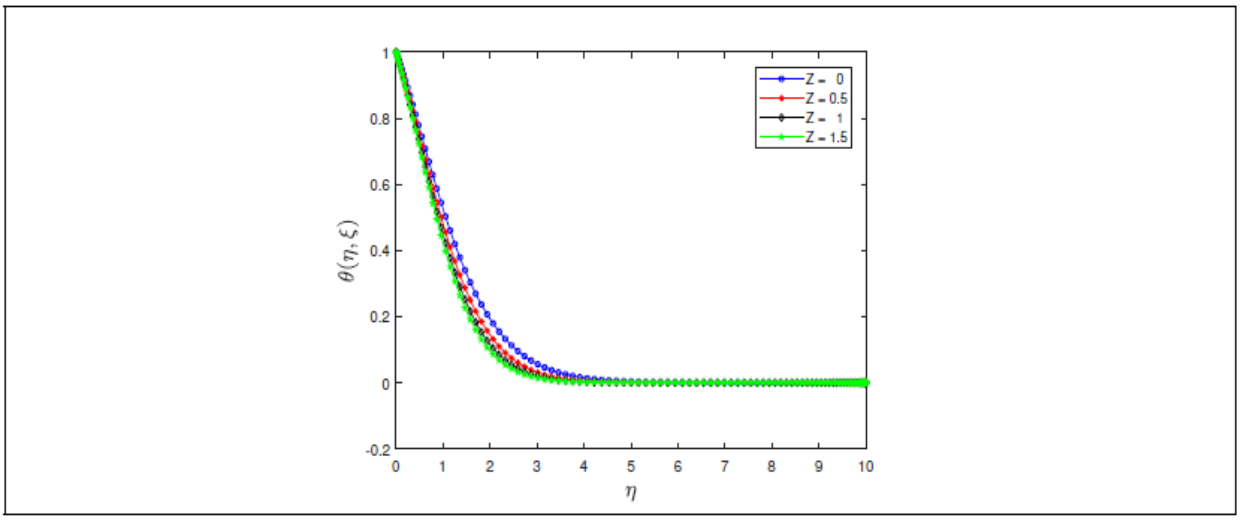

Figure 9: Effect of modified Hartmann number on the temperature profile when $\beta = 2, \delta = 0.5, \epsilon = 0.1, Pr = 1; Nb = Nt = 0.3, Le = 5$ and $Ec = 0.1$.

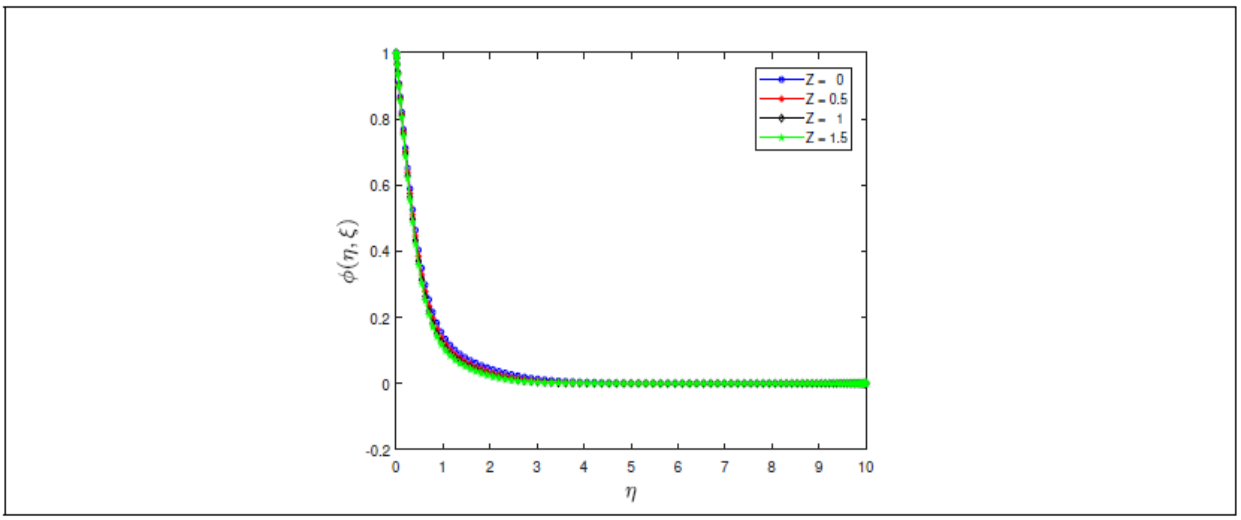

Figure 10: Effect of modified Hartmann number on the concentration profile when $\beta = 2, \delta = 0.5, \epsilon = 0.1, Pr = 1; Nb = Nt = 0.3, Le = 5$ and $Ec = 0.1$.

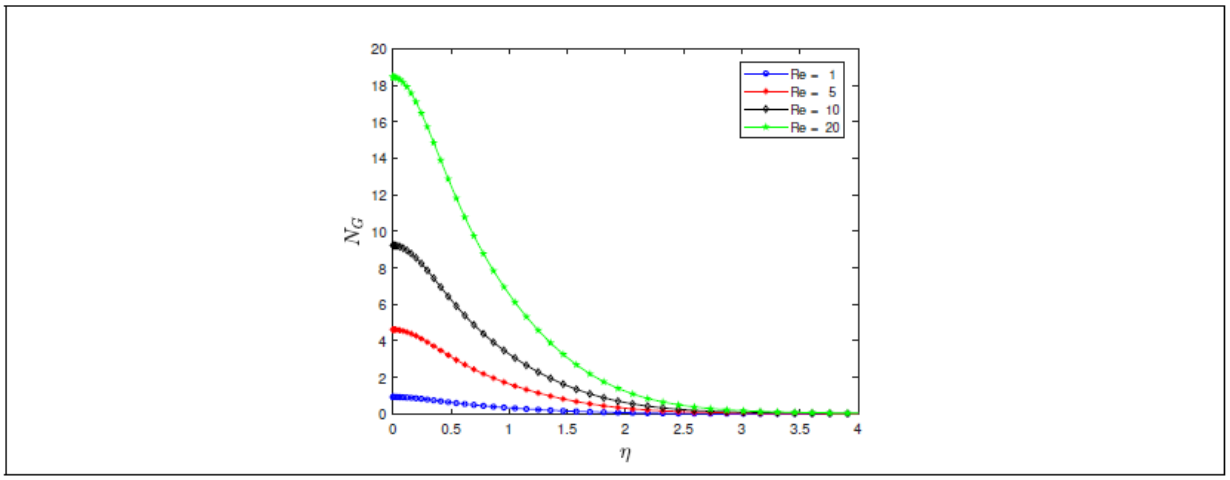

Figure 11: Entropy generation number for different values of the Reynold's number when $Br = 0.5, \Omega = 1, Re = 10$, and $\lambda_1 = 0.5$.

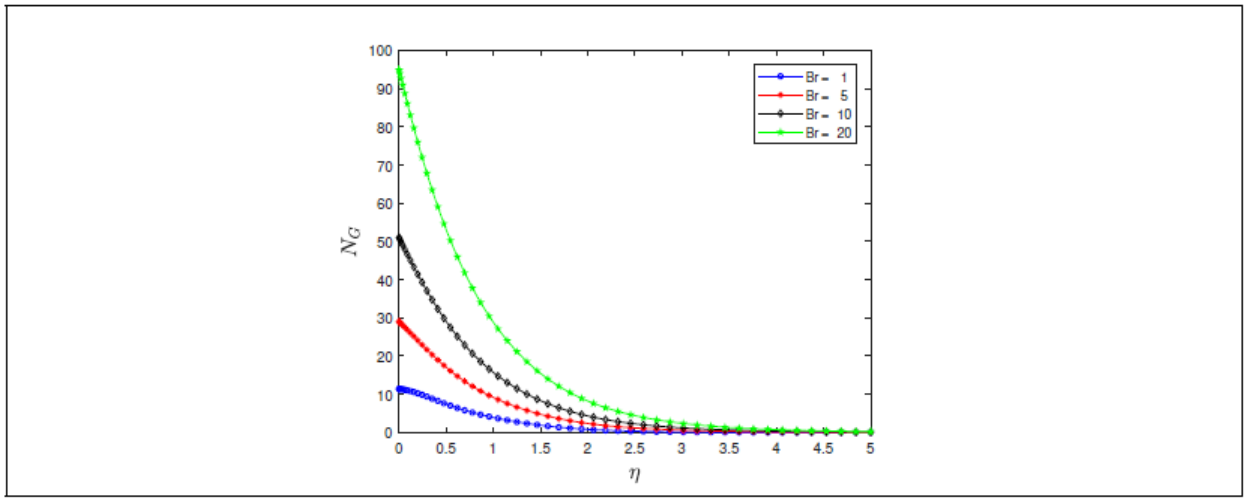

Figure 12: Entropy generation number for different values of the Brinkmann number when $Br = 0.5, \Omega = 1, Re = 10$, and $\lambda_1 = 0.5$.

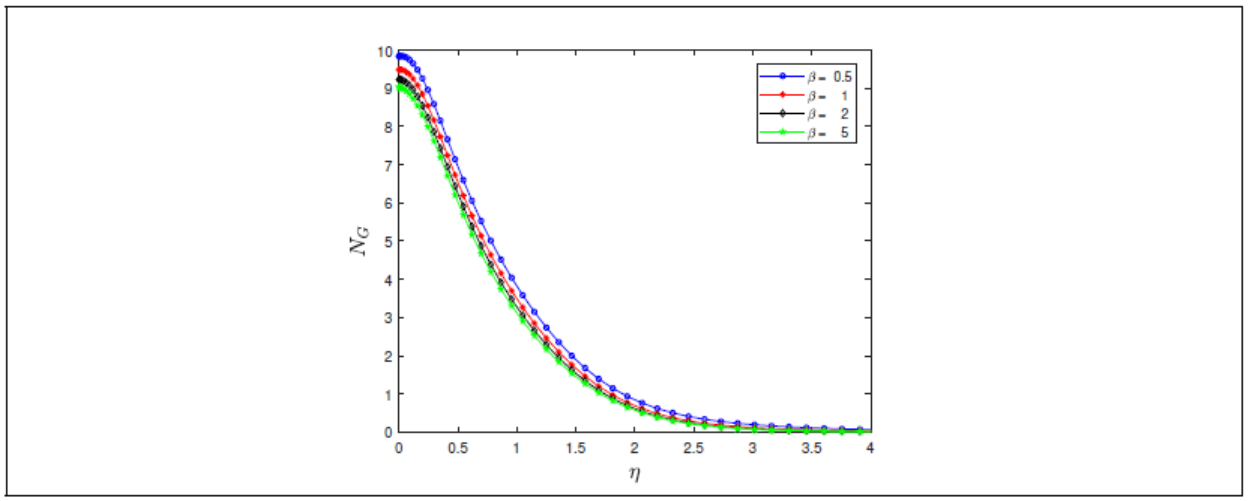

Figure 13: Entropy generation number for different values of the Casson parameter when $Br = 0.5, \Omega = 1, Re = 10$, and $\lambda_1 = 0.5$.

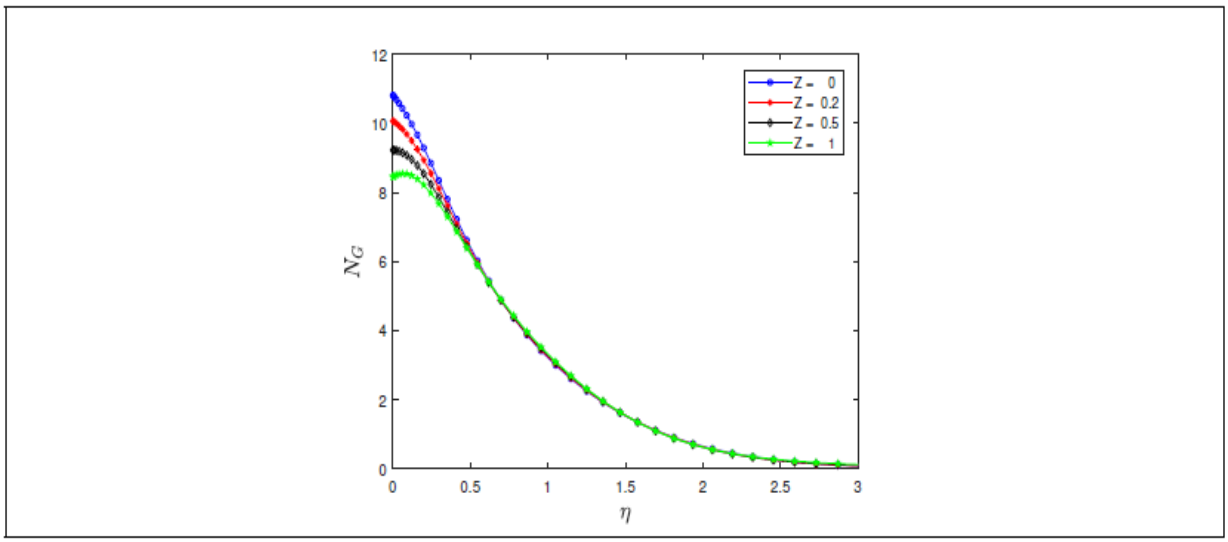

Figure 14: Entropy generation number for different values of the modified Hartmann number when $Br = 0.5, \Omega = 1, Re = 10$, and $\lambda_1 = 0.5$.

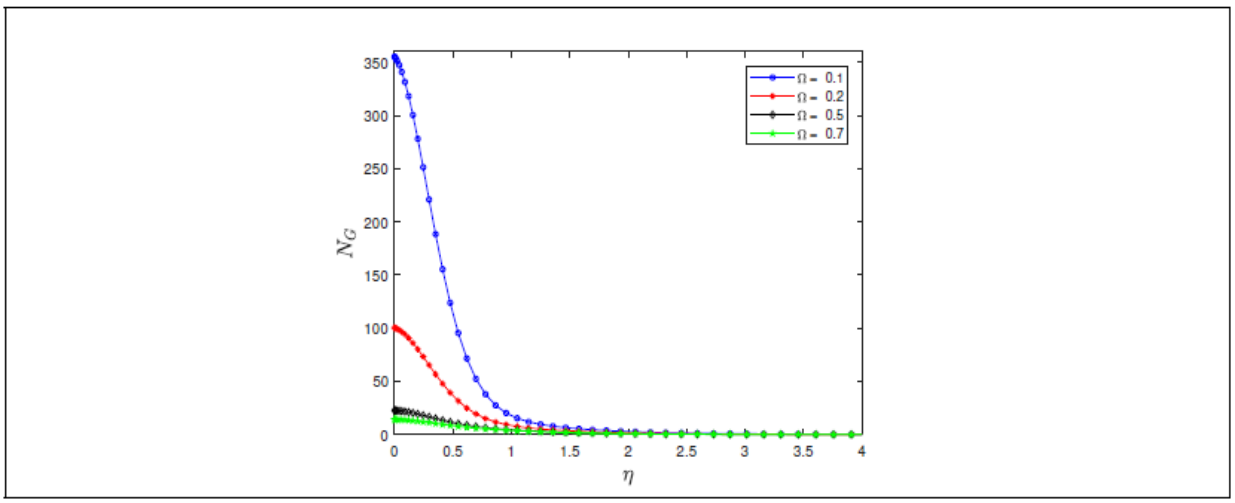

Figure 15: Entropy generation number for different values of the dimensionless temperature when $Br = 0.5, \Omega = 1, Re = 10$, and $\lambda_1 = 0.5$.

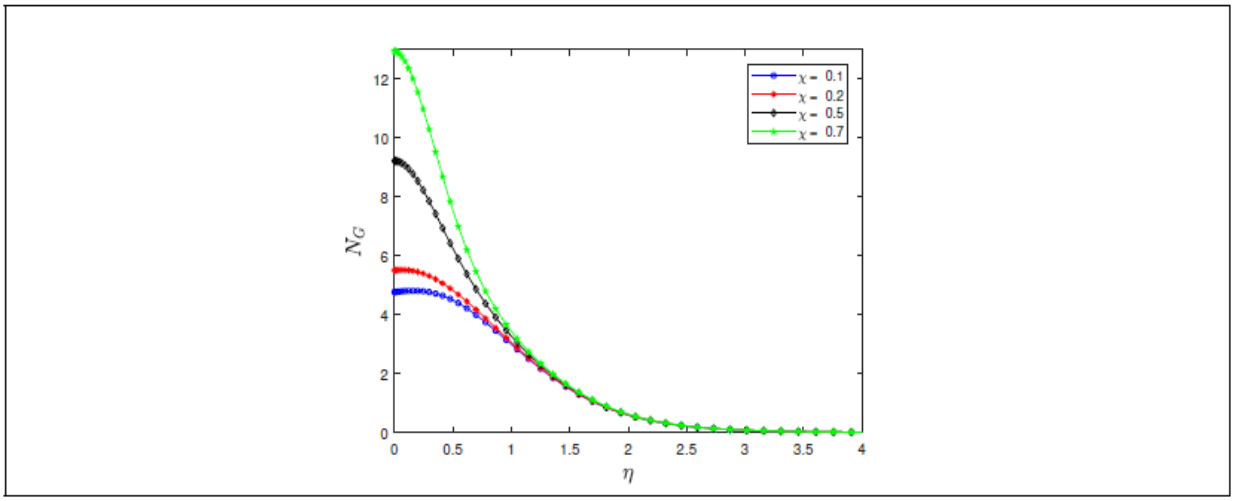

Figure 16: Entropy generation number for different values of the dimensionless concentration when $Br = 0.5, \Omega = 1, Re = 10$, and $\lambda_1 = 0.5$.

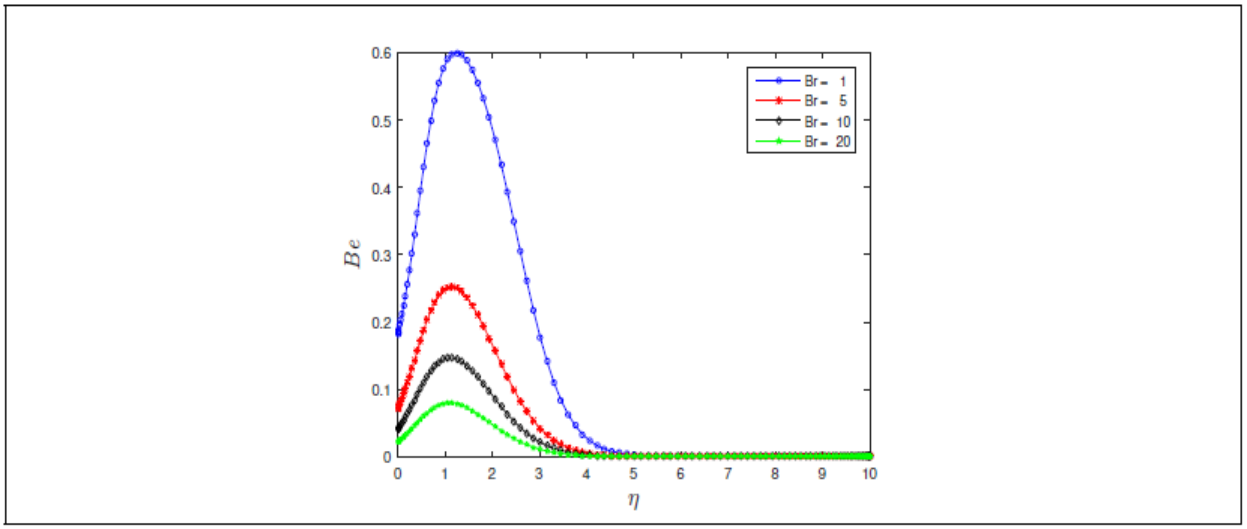

Figure 17: Bejan number for different values of the Brinkmann number.

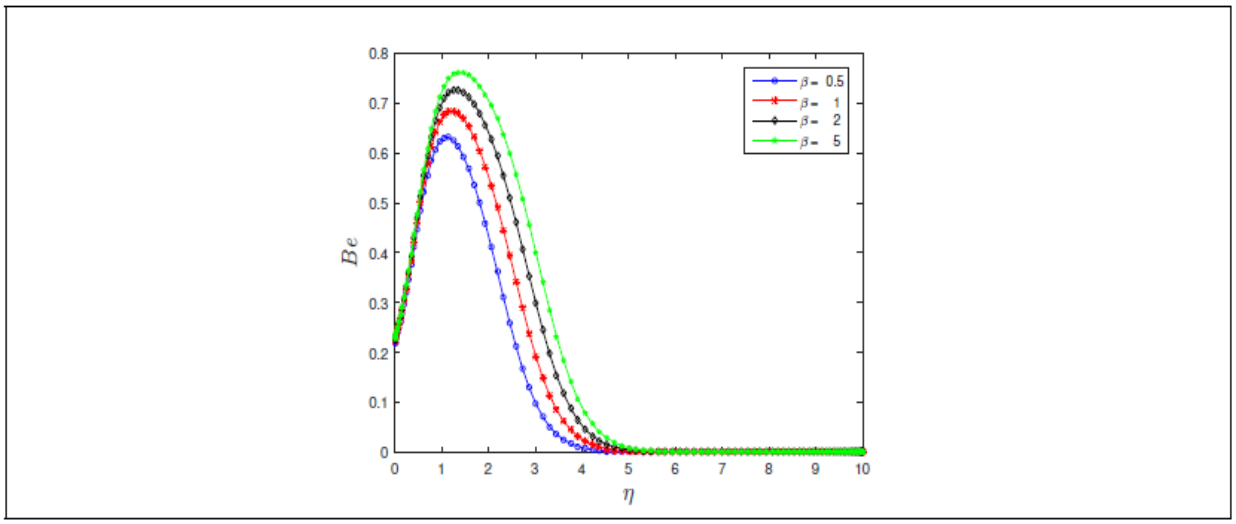

Figure 18: Bejan number for different values of the Casson parameter.

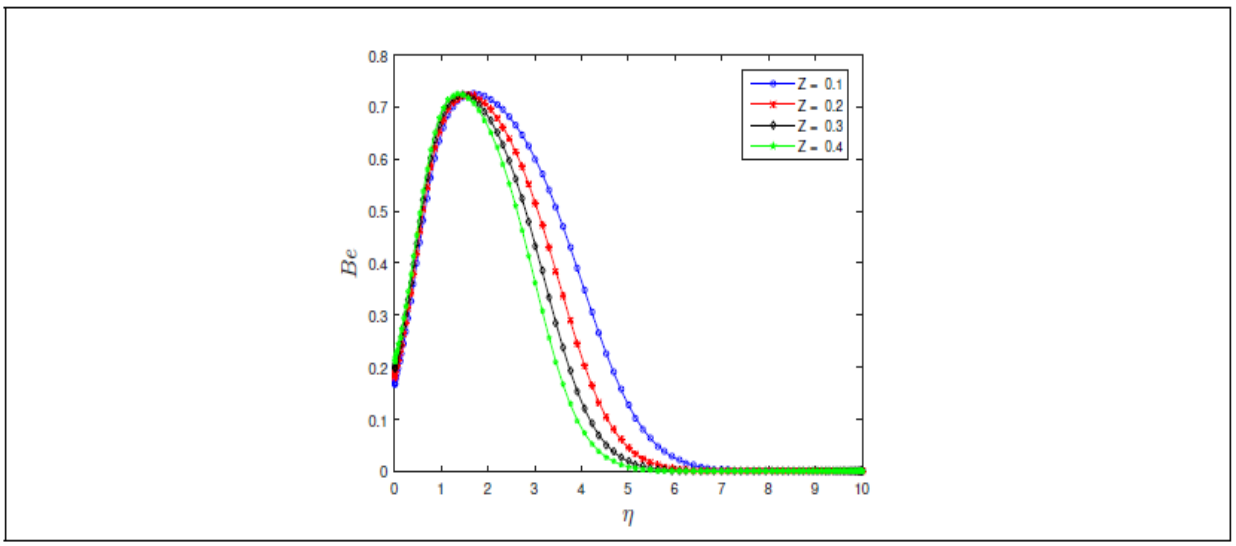

Figure 19: Bejan number for different values of the modified Hartmann number.

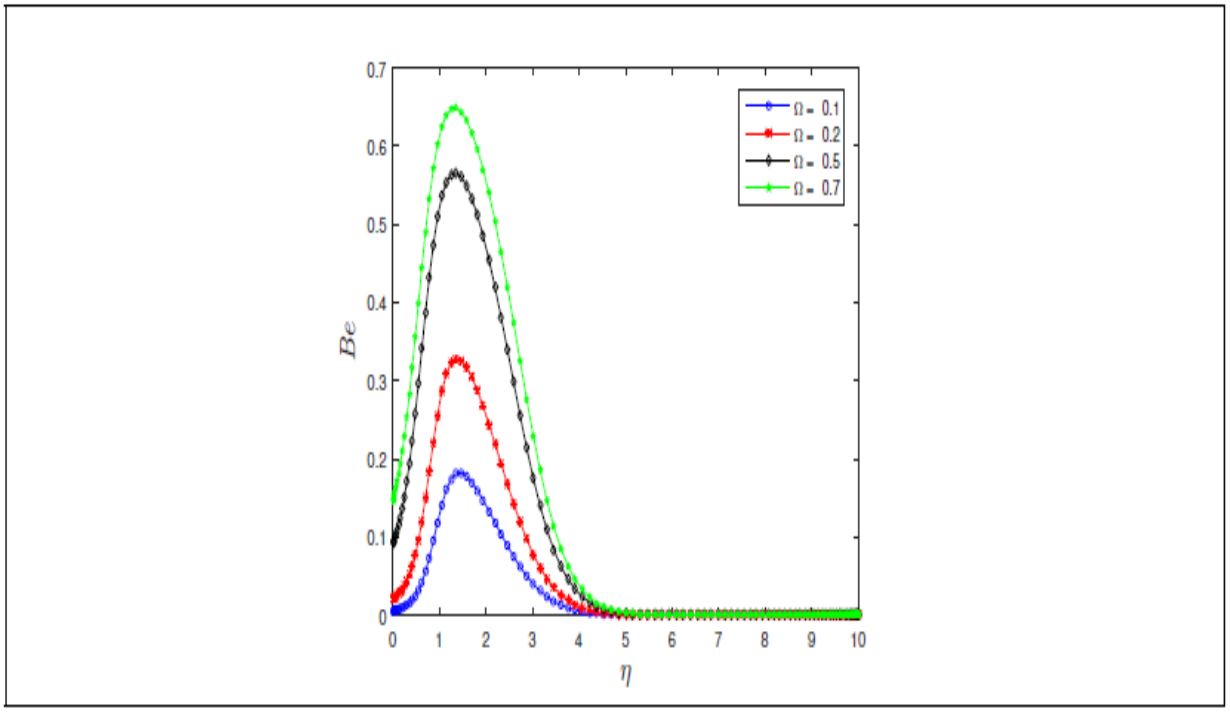

Figure 20: Bejan number for different values of the dimensionless temperature.

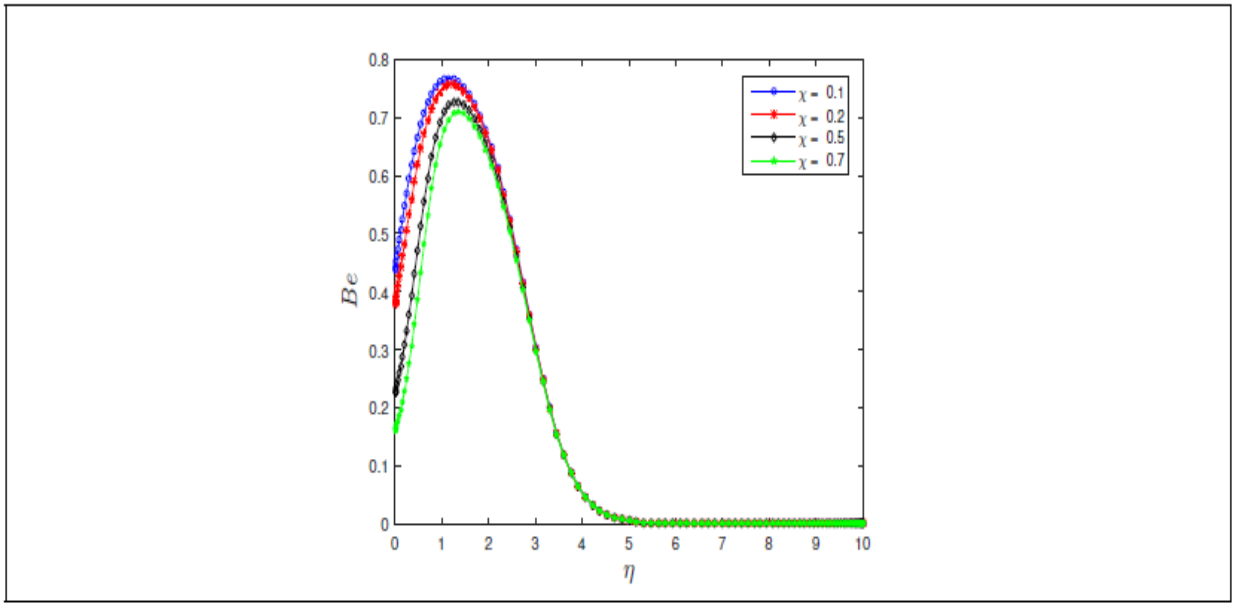

Figure 21: Bejan number for different values of the dimensionless concentration.

Conclusions: -

The flow heat and mass transfer of a Casson nanofluid past an electromagnetic stretching Riga plate have been analyzed by us. The effect of entropy generation, viscous dissipation, Brownian motion, and thermophoresis diffusion is considered by the problem. The results, which are obtained in the study, are summarized as follows:

1. When the Casson parameter increases, velocity profile decreases, while for increasing values of the modified Hartmann number, it increases.

2. When the velocity ratio parameter is less than unity, velocity profile increases. But if the velocity ratio parameter values greater than unity, it decreases.

3. When the Casson parameter increases, temperature and concentration profile increase. But when the velocity ratio parameter and Modified Hartmann number are increased, the profiles decrease.

4. When the Brinkmann number increases, entropy generation increases.

5. When the modified Hartmann number increases, entropy generation decreases.

6. When the value of the dimensionless concentration increases, entropy generation increases.

References: -

[1] T. Abbas, M. Ayub, M. Bhatti, M. Rashidi & M. Ali (2016). Entropy generation on nanofluid flow through a horizontal Riga plate. Entropy, 18(6), 223.

[2] M. H. Abolbashari, N. Freidoonimehr, F. Nazari & M. M. Rashidi (2015). Analytical modeling of entropy generation for Casson nano-fluid flow induced by a stretching surface. Advanced Powder Technology, 26(2), 542–552.

[3] A. Ahmad, S. Asghar & S. Afzal (2016). Flow of nanofluid past a Riga plate. Journal of Magnetism and Magnetic Materials, 402, 44–48.

[4] R. Ahmad, M. Mustafa&M. Turkyilmazoglu (2017). Buoyancy effects on nanofluid flowpast a convectively heated vertical Riga-plate: A numerical study. *International Journal of Heat and Mass Transfer*, *111*, 827–835.

[5] M. Atlas, S. Hussain & M. Sagheer (2018). Entropy generation and squeezing flow past a Riga plate with Cattaneo-Christov heat flux. *Bulletin of the Polish Academy of Sciences: Technical Sciences*, *66*(3), 291–300.

[6] J. Buongiorno (2006). Convective transport in nanofluids. Journal of Heat Transfer, 128, 240– 250.

[7] C. Canuto, M. Y. Hussaini, A. Quarteroni & T. A. Zhang (1988). Spectral methods in fluid dynamics. Springer, Berlin, Heidelberg.

[8] S. Choi (1995). Ehnancing thermal conductivity of fluids with nanoparticles. ASME, 231, 99–106.

[9] M. Das, G. Mahanta & S. Shaw (2020). Heat and mass transfer effect on an unsteady MHD radiative chemically reactive Casson fluid over a stretching sheet in porous medium. Heat Transfer, 49(8), 4350–4369.

[10] S. K. Das, S. U. S. Choi & H. E. Patel (2006). Heat transfer in nanofluids - A review. Heat Transfer Engineering, 27(10), 3–19.

[11] R. Dash, K. Mehta & G. Jayaraman (1996). Casson fluid flow in a pipe filled with a homogeneous porous medium. International Journal of Engineering Science, 34(10), 1145–1156.

[12] A. Gailitis & O. Lielausis (1961). On the possibility to reduce the hydrodynamic resistance of a plate in aelectro-lyte. Applied Magnetohydrodynamics, 12, 143–146.

[13] Y. Gupta, P. Rana, O. Beg & A. Kadir (2020). Multiple solutions for slip effects on dissipative magneto-nanofluid transport phenomena in porous media: Stability analysis. Journal of Applied and Computational Mechanics, 6(4), 956–967.

[14] A. Hakeem, P. Ragupathi, S. Saranya & B. Ganga (2020). Three dimensional non-linear radiative nanofluid flow over a Riga plate. Journal of Applied and Computational Mechanics, 6(4), 1012–1029.

[15] M. Hamad (2011). Analytical solution of natural convection flow of a nanofluid over a linearly stretching sheet in the presence of magnetic field. International Communications in Heat and Mass Transfer, 38(4), 487–492.

[16] T. Hayat, T. Abbas, M. Ayub, M. Farooq & A. Alsaedi (2016). Flow of nanofluid due to convectively heated Riga plate with variable thickness. Journal of Molecular Liquids, 222, 854– 862.

[17] T. Hussain, S. Shehzad, A. Alsaedi, T. Hayat & M. Ramzan (2015). Flow of casson nanofluid with viscous dissipation and convective conditions- A mathematical model. Journal of Central South University, 22, 1132–1140.

[18] W. Khan & I. Pop (2010). Boundary layer flow of a nanofluid past a stretching sheet. International Journal of Heat and Mass Transfer, 53(11-12), 2477–2483.

[19] A. Kumar, R. Tripathi, R. Singh & M. Sheremet (2021). Entropy generation on double diffusive MHD Casson nanofluid flow with convective heat transfer and activation energy. Indian Journal of Physics, 95, 1423–1436.

[20] A. Kunetsov & D. Nield (2014). Natural convective boundary layer flow of a nanofluid past a vertical plate: A revised model. International Journal of Thermal Sciences, 77, 126–129.